MAGNETISM

All-oxide–based synthetic antiferromagnets exhibiting layer-resolved magnetization reversal

Binbin Chen,[1,2] Haoran Xu,[1] Chao Ma,[1] Stefan Mattauch,[3] Da Lan,[1] Feng Jin,[1,2] Zhuang Guo,[1] Siyuan Wan,[1] Pingfan Chen,[1] Guanyin Gao,[1] Feng Chen,[2] Yixi Su,[3] Wenbin Wu[1,2,4]*

Synthesizing antiferromagnets with correlated oxides has been challenging, owing partly to the markedly degraded ferromagnetism of the magnetic layer at nanoscale thicknesses. Here we report on the engineering of an antiferromagnetic interlayer exchange coupling (AF-IEC) between ultrathin but ferromagnetic $La_{2/3}Ca_{1/3}MnO_3$ layers across an insulating $CaRu_{1/2}Ti_{1/2}O_3$ spacer. The layer-resolved magnetic switching leads to sharp steplike hysteresis loops with magnetization plateaus depending on the repetition number of the stacking bilayers. The magnetization configurations can be switched at moderate fields of hundreds of oersted. Moreover, the AF-IEC can also be realized with an alternative magnetic layer of $La_{2/3}Sr_{1/3}MnO_3$ that possesses a Curie temperature near room temperature. The findings will add functionalities to devices with correlated-oxide interfaces.

Over the past few decades, antiferromagnets (AFMs) have been frequently used in magnetic devices in auxiliary roles—for example, as pinning layers to harden the operating ferromagnetic (FM) layers in spin valves and magnetic tunnel junctions (*1*). Lately, with the development of probes and manipulations on the magnetic state in AFMs, such as atomic-scale spin-polarized tunneling and electric-current–induced spin transfer torque (*2*, *3*), concepts of memory devices based directly on AFMs have been demonstrated (*4*). Compared with the ferromagnets, AFMs have the advantage of insensitivity to disturbing magnetic fields, while producing no stray fields.

Synthetic antiferromagnets (S-AFMs) are built with FM layers periodically interleaved with metallic or insulating spacers, where the magnetization of adjacent FM layers alternates owing to the antiferromagnetic (AF) interlayer exchange coupling (IEC). For metallic spacers, IEC is achieved via a RKKY (Ruderman-Kittel-Kasuya-Yosida)–type exchange interaction mediated by spin-polarized charge carriers in the spacer. The coupling strength is found to oscillate and change sign with the spacer thickness, and the oscillation periods are determined by the Fermi surface topology of the spacer (*5*). For insulating spacers like MgO, the IEC depends on the spin-polarized tunneling, and the strength decays exponentially with the spacer layer thickness (*6*, *7*). Unlike bulk AFMs with huge exchange fields, the S-AFMs have a comparable magnitude of IEC and Zeeman energy, which makes them well-suited for investigating the field-induced magnetic switching in AFMs, such as the surface spin-flop transition and the domain wall dynamics (*8*, *9*). Moreover, the S-AFMs with giant magnetoresistance effect have been widely used in magnetic sensors and magnetoresistive random access memories (*1*). With the increasing demand for high-density storage, three-dimensional memories based on perpendicularly magnetized S-AFMs have also been experimentally demonstrated, including the racetrack and ratchetlike memories (*10*, *11*). However, in contrast to these achievements in S-AFMs composed of transition metals and alloys, the layer-resolved magnetic switching in S-AFMs with correlated-oxide multilayers has rarely been observed (*9*, *11*–*15*).

To achieve the AF-IEC in correlated-oxide multilayers, epitaxial growth with atomic-layer control is required and at the same time, the ferromagnetism of the FM layers needs to be maintained at nanoscale thicknesses. Although the advances in film growth have enabled the discovery of many intriguing phenomena at oxide interfaces (*14*–*16*), the thickness-dependent degradation of ferromagnetism in magnetic oxide films seems ubiquitous. This "dead layer" effect can be one of the major obstacles to the development of all-oxide S-AFMs. When scaled down to nanometer thicknesses, for example, the manganite films show a rapidly decreased Curie temperature (T_C) (*17*–*21*), and for $La_{2/3}Ca_{1/3}MnO_3$ (LCMO), the magnetic dead layer is at least eight unit-cells thick (*20*). Much effort has been devoted to attenuating this effect, such as inserting buffer layers to control the interfacial electronic reconstructions or modulating the epitaxial strain states via interfacial octahedral coupling (*17*, *18*). Recently, heterostructuring with metallic ruthenates was shown to be effective because the interfacial interactions from the ruthenates seem less disruptive for the double exchange at the manganite interfaces (*19*–*21*).

Here, we constructed S-AFMs using LCMO as the magnetic layers, $CaRu_{1/2}Ti_{1/2}O_3$ (CRTO) as the spacer layers, and (001)-oriented $NdGaO_3$ (NGO) as the substrate. Bulk LCMO is a half-metallic ferromagnet with a T_C of 265 K, and its nearly 100% spin polarization at the Fermi level makes it highly promising for spintronic device applications (*22*, *23*). By contrast, bulk CRTO, derived from the paramagnetic metal $CaRuO_3$ (CRO), is a semiconductor at all temperatures with a weak ferromagnetism below ~38 K (*24*). Ultrathin CRTO films, however, are insulating and show negligible magnetism in the whole temperature range (fig. S1). Notably, both component layers share the same *Pbnm* structure with the NGO substrate. Under the same symmetry and with comparable lattice constants (*25*), the heterostructures show excellent epitaxial growth with atomically flat surfaces and interfaces (fig. S2), which is found to be a prerequisite for the AF-IEC. Meanwhile, the dominant magnetostriction energy caused by a tensile strain along the [010] axis (all in orthorhombic index hereafter) provides the LCMO layers a robust in-plane uniaxial magnetic anisotropy (MA), with the easy-axis also along the [010] (*25*–*27*). The combination of AF-IEC with the MA leads to a soft and sensitive response of the magnetization configurations to external magnetic fields.

The LCMO/CRTO multilayers $[x/y]_N$ are grown by pulsed laser deposition, with x (y) denoting the LCMO (CRTO) thickness in nanometers and N the repetition number of the bilayers (*25*). They all start with CRTO, and to keep an identical interfacial arrangement for each LCMO layer, the top LCMO layer is also capped with one more CRTO layer at the same thickness (y). Figure 1A shows the magnetic properties of a representative LCMO/CRTO superlattice (SL), $[2.8/1.2]_{10}$. It displays a T_C of 182 K, greatly enhanced compared with the plain LCMO film at 2.8 nm (*20*) but lower than the corresponding LCMO/CRO SL (T_C ~ 265 K), which is fabricated for comparison. The difference in T_C of the two SLs can be ascribed to a relatively weakened electron leakage at the LCMO/CRTO interfaces caused by the depletion of Ru 4d band by Ti doping (*19*). Notably, the LCMO/CRTO SL shows a decrease of moments at 140 K, also in sharp contrast to the LCMO/CRO SL. Given the negligible magnetism in ultrathin CRTO films (fig. S1), such a drop in magnetization is recognized as a signature of the AF-IEC between FM LCMO layers across the CRTO spacers. This assertion can be confirmed by the hysteresis loops shown in the inset of Fig. 1A. Although the LCMO/CRO SL shows an almost square loop, the LCMO/CRTO SL shows a negligible M_R with M_R/M_S ~ 3%, where M_R (M_S) is the remanent (saturation) magnetization. Moreover, the loop exhibits multiple discrete steps with two magnetization plateaus at ~ $\pm 1/5 M_S$ (for a full set of loops at various temperatures, see fig. S5), which provides concrete evidence for the AF-IEC in the LCMO/CRTO SL.

[1]Hefei National Laboratory for Physical Sciences at Microscale, University of Science and Technology of China, Hefei 230026, China. [2]Anhui Key Laboratory of Condensed Matter Physics at Extreme Conditions, High Magnetic Field Laboratory, Chinese Academy of Sciences, Hefei 230031, China. [3]Juelich Centre for Neutron Science (JCNS) at the Heinz Maier-Leibnitz Zentrum (MLZ), Forschungszentrum Juelich GmbH, D-85747 Garching, Germany. [4]Collaborative Innovation Center of Advanced Microstructures, Nanjing University, Nanjing 210093, China.
*Corresponding author. Email: wuwb@ustc.edu.cn

Downloaded from http://science.sciencemag.org/ on April 23, 2020

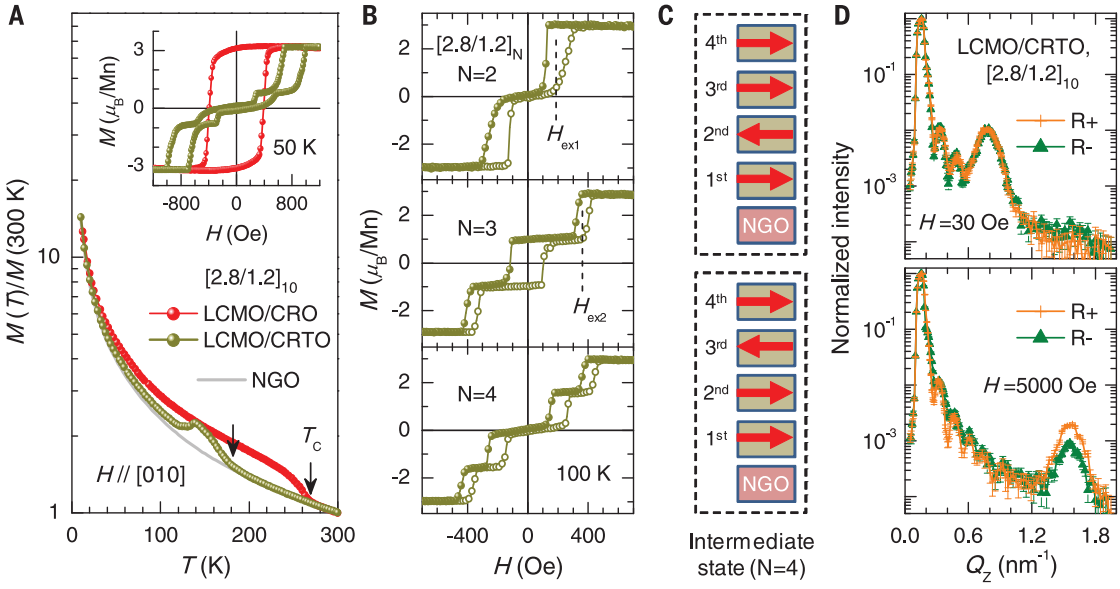

Fig. 1. AF-IEC in LCMO/CRTO multilayers. (**A**) Temperature (T) dependence of normalized magnetization (M) measured in LCMO/CRTO and LCMO/CRO SLs, $[2.8/1.2]_{10}$. The paramagnetic background from the NGO(001) substrates is included for comparison. During these measurements, a cooling field of 250 Oe is applied along the in-plane easy-axis [010]. The inset shows the corresponding hysteresis loops measured at 50 K from each SL, with the paramagnetic background from the NGO substrate subtracted (figs. S3 and S4). (**B**) Hysteresis loops measured at 100 K from LCMO/CRTO SLs, $[2.8/1.2]_N$, with N = 2, 3, and 4, respectively. For clarity, the steplike loop measured with the magnetic field (H) sweeping from positive (negative) to negative (positive) is denoted with solid (open) circles (fig. S6). (**C**) Two possible magnetic configurations of the intermediate state for the N = 4 SL, which has the magnetization plateau at $1/2M_S$. (**D**) PNR measured at 10 K from LCMO/CRTO SL, $[2.8/1.2]_{10}$, with the field of 30 Oe (top) or 5000 Oe (bottom) applied along the in-plane easy-axis [010].

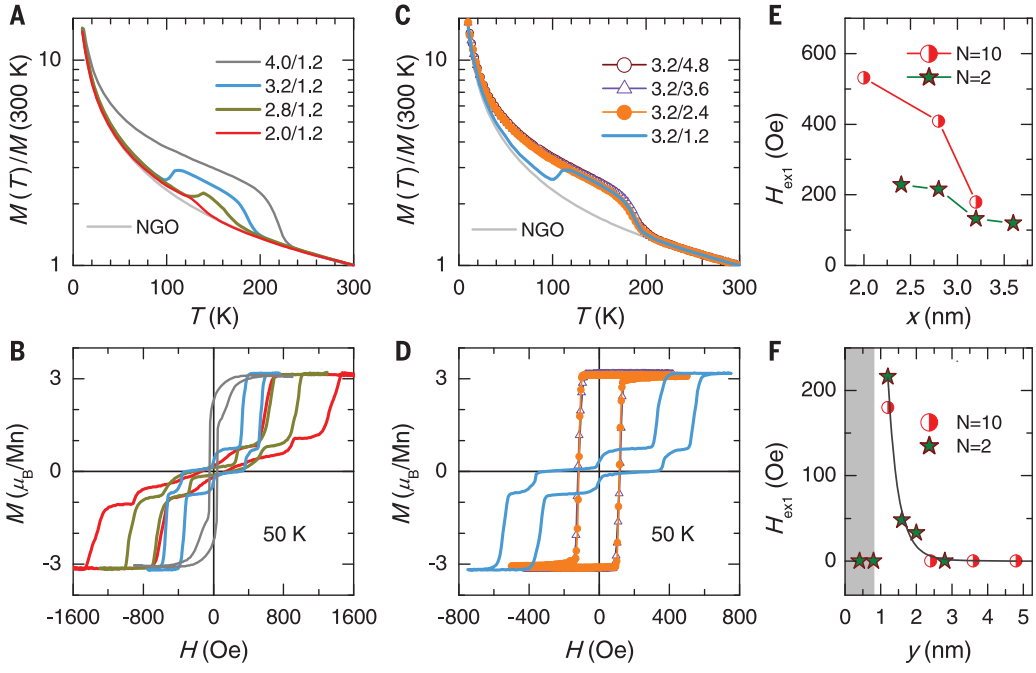

Fig. 2. Dependence of IEC on layer thicknesses. Normalized M-T curves and M-H hysteresis loops measured from the LCMO/CRTO SLs, $[x/1.2]_{10}$, with varying LCMO thicknesses (**A** and **B**) and $[3.2/y]_{10}$ with varying CRTO thicknesses (**C** and **D**). During the measurements, the field is applied along the in-plane easy-axis [010]. For the M-T curves, the cooling field is set at 250 Oe, and for each hysteresis loop, the paramagnetic background from the NGO substrate is subtracted. (**E**) The exchange field H_{ex1} plots against the LCMO thickness (x) extracted from (B); the data measured at 100 K for the N = 2 SLs are also shown. Lines are guides to the eye. (**F**) H_{ex1} plots against the CRTO thickness (y) extracted from (D); the data measured at 100 K for the N = 2 SLs (x = 2.8 nm) are also shown. For the samples with FM-like hysteresis loops, H_{ex} is set at zero. The solid line is an exponential fitting to the data extracted from the N = 2 SLs.

To explain the magnetization plateaus, we first examine the magnetic switching behavior in LCMO/CRTO SLs, $[2.8/1.2]_N$, with increasing N (Fig. 1B). The results are in good agreement with the Monte Carlo simulations performed for the prototype perpendicularly magnetized S-AFMs, where only the nearest-neighbor interactions were considered (*28*). In (*28*), the magnetization of each FM layer was modeled as a classic Ising spin (S = ±1), and this is also satisfied by our system, considering the abrupt magnetization reversal and strong uniaxial MA (fig. S7). For N = 2, as the magnetic field is swept, apart from the plateaus $\pm M_S$, one more magnetization step at $M_R \sim 0$ is observed corresponding to the antiparallel magnetic alignments of the two LCMO layers. Defining the exchange field H_{ex1} as the offset of the separated loops from zero field, the IEC strength can be calculated as $J = xM_SH_{ex1}$ = 0.025 erg/cm^2, which is nearly two orders of magnitude smaller than that of the transition-metal multilayers (*29*). For N = 3, the central LCMO layer can receive interactions from the two outer LCMO layers, yielding the separated loops centered at $H_{ex2} \sim 2H_{ex1}$. The steps at $M_R \sim \pm 1/3M_S$ originate from a single LCMO layer uncompensated in the AF state (fig. S8A). For N = 4,

Downloaded from http://science.sciencemag.org/ on April 23, 2020

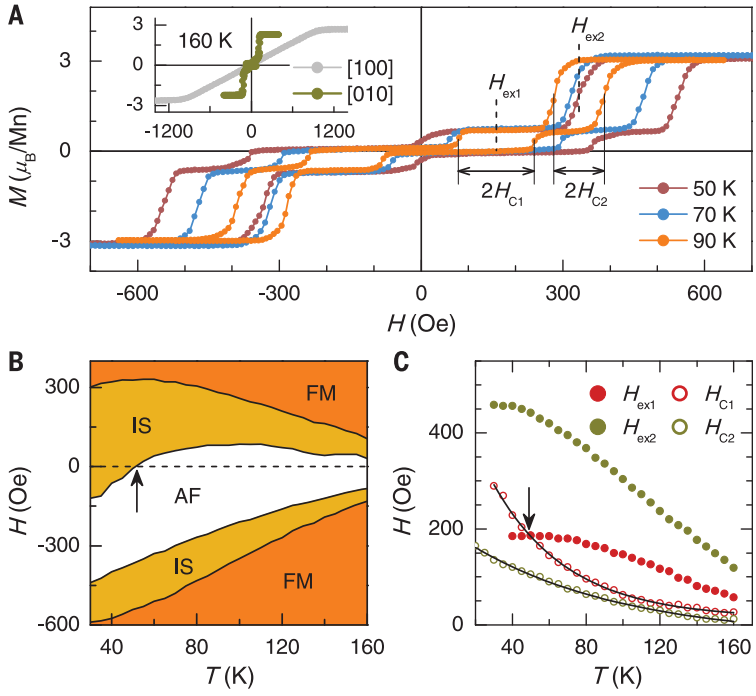

Fig. 3. Temperature-dependent magnetization reversal in LCMO/CRTO SL. (**A**) *M-H* hysteresis loops measured from the LCMO/CRTO SL, $[3.2/1.2]_{10}$, with the temperature fixed at 50, 70, and 90 K. H_{ex1} (H_{ex2}) and H_{C1} (H_{C2}) correspond to the coupling field and coercivity of the outer (interior) LCMO layers. The inset shows the loops measured at 160 K with the field applied along the in-plane [010] and [100] directions, respectively. (**B**) Magnetic configurations mapped at various temperatures and magnetic fields for the $[3.2/1.2]_{10}$ SL, where "FM" denotes the parallel magnetic alignments of all LCMO layers, "IS" is an intermediate state with antiparallel alignments of all the interior LCMO layers but parallel alignments of the two outer LCMO layers, and "AF" means antiparallel alignments of all adjacent LCMO layers (Fig. 1C and fig. S11). The horizontal line indicates the remanent states at various temperatures. (**C**) The temperature dependence of H_{ex1} (H_{ex2}) and H_{C1} (H_{C2}), with the coercivity exponentially fitted. The arrow in (B) and (C) marks a crossover from AF state to IS.

considering the identical exchange interactions for the 2nd and 3rd LCMO layers (from bottom to top), when swept from positive to negative saturation fields, two possible layer-resolved magnetic switching sequences can be adopted, i.e., 2nd-4th-1st-3rd or 3rd-1st-4th-2nd (fig. S8B). This leads to an intermediate state (IS), with the plateau at ~ $+1/2M_S$ and, correspondingly, two possible magnetic configurations (Fig. 1C). Analogously, the magnetization plateaus at ~ $\pm1/5M_S$ for the N = 10 SL can be assigned to the IS after switching the four interior LCMO layers (2nd, 4th, 6th, 8th) or (3rd, 5th, 7th, 9th) from a fully saturated state. Notably, the magnetization reversal shown for these all-oxide S-AFMs bears almost the same features as the perpendicularly magnetized metal and alloy systems (*28*, *30*).

To directly demonstrate the AF-IEC in these SLs, we performed polarized neutron reflectivity (PNR) measurements (*25*) on the LCMO/CRTO SL, $[2.8/1.2]_{10}$, as shown in Fig. 1D. At a low field of 30 Oe, both the spin-up (R^+) and spin-down (R^-) polarized neutrons show reflections at Q_Z = 0.78 nm^{-1} (*25*), leaving a periodicity of twice the bilayer thickness (8 nm). Such a magnetic periodicity can only be explained by the AF-IEC in the SL (*31*). At 5000 Oe, these reflections are fully suppressed, and new ones appear at exactly the structural Bragg peak at Q_Z = 1.57 nm^{-1}, indicating the transition from antiparallel to parallel magnetic alignments of all the LCMO layers. Further, in Fig. 1, it is noted that all the SLs, including the LCMO/CRO SL, have nearly equal values of M_S (which is normalized to the LCMO volume only), implying that the moments of the SLs are predominantly determined by the LCMO layers and the steplike switching cannot be attributed to the interfacial exchange coupling (*19*, *32*). Also, given the in-plane magnetization, stepwise hysteresis loops, large lateral dimensions (*25*), flat interfaces, and that the coupling strength falls off rapidly with the CRTO thickness (shown later), the AF-IEC cannot be controlled by the interlayer dipolar coupling (*30*). Instead, the spin-polarized tunneling across the CRTO spacer may play a major role. The Ti/Ru doping can not only retain a high T_C in the LCMO layers, but also leave defects at the interfaces or in the spacer. As has been pointed out, the localized defect or impurity states could make the IEC become AF and substantially stronger compared to a perfect tunneling barrier (*33*).

After establishing the AF-IEC in LCMO/CRTO SLs, we turn to examine its dependence on the layer thickness. For the LCMO layer (Fig. 2A), as x is reduced from 4.0 to 2.0, the T_C of the SLs decreases steadily from 229 to 150 K. Such a finite-size effect is generally observed for FM oxide films, although the heterostructuring with ruthenates has made the degradation here rather moderate (*19*–*21*). All the SLs show a drop in magnetization below the T_C except the one with x = 4.0. Correspondingly, all the SLs with thinner LCMO show an AF state with well-defined magnetization plateaus at ~ $\pm1/5M_S$, whereas the one with x = 4.0 shows M_R/M_S ~ 73% (Fig. 2B). The exchange field H_{ex1} increases with decreasing x (Fig. 2E). For SL with x = 4.0, the IEC is FM-like. A similar trend is observed for the N = 2 series (fig. S9A). Actually, it has been proposed that for transition-metal S-AFMs, the AF-IEC occurs only at the interfaces across the nonmagnetic spacer, and the coupling strength (J) should not depend on the FM layer thickness x, leaving H_{ex1} (H_{ex2}) $\propto x^{-1}$ (*7*, *34*). This is in agreement with our observations, and the deviation may arise from the finite-size effect in LCMO layers.

For the CRTO spacer, as shown in Fig. 2, C and D, at y > 1.2, all the SLs exhibit a FM behavior with almost the same temperature- and field-dependent magnetizations. However, at y = 1.2, the AF-IEC appears. With x fixed at 3.2, all the SLs show the same T_C ~ 200 K, suggesting that the different IEC may contribute little to T_C. These observations also indicate that the magnetization of the SLs is dominated by the LCMO layers. For ultrathin CRTO with y = 0.8 and 0.4, the FM-IEC dominates over the intrinsic AF-IEC because of possible pinholes, as expected (*7*). Similar results are obtained from the N = 2 SLs as summarized in Fig. 2F (fig. S9B), where the AF-IEC strength also peaks at y = 1.2. We observe a rapid damping of H_{ex1} (H_{ex2}) in the thickness range of y = 1.2 to 2.0, but the existence of the oscillatory coupling observed commonly for metallic S-AFMs cannot be claimed in our system. We expect that the coupling is controlled by the spin-polarized tunneling as suggested for the Fe/MgO/Fe system (*7*, *33*), where the coupling strength decays exponentially with increasing spacer thicknesses owing to the evanescent electron waves (*6*). H_{ex1} of the N = 2 series at various values of y (Fig. 2F) can be well fitted with an exponential law $H_{ex1} \propto y^{-2}\exp(-y/\lambda)$ predicted by the quantum interference model (*6*), with a decay length λ = 0.5 nm. Therefore, such a damping is consistent with the insulating nature of the ultrathin CRTO spacer.

We now move to the temperature-dependent magnetic switching and AF-IEC in this system. A full set of hysteresis loops measured from an optimized SL, $[3.2/1.2]_{10}$, are shown in fig. S10. For an in-plane magnetized film, the magnetic switching is usually controlled by the competition between AF-IEC and MA (*35*). In the inset of Fig. 3A, the loops measured with the magnetic field applied along the two orthogonal in-plane axes signify a typical uniaxial MA, with the easy-axis along [010] and the hard-axis along [100] (fig. S7) (*27*). At 160 K, the anisotropy field H_{MA} ~ 950 Oe, deduced from the saturation field in the [100] direction, is much larger than the

Downloaded from http://science.sciencemag.org/ on April 23, 2020

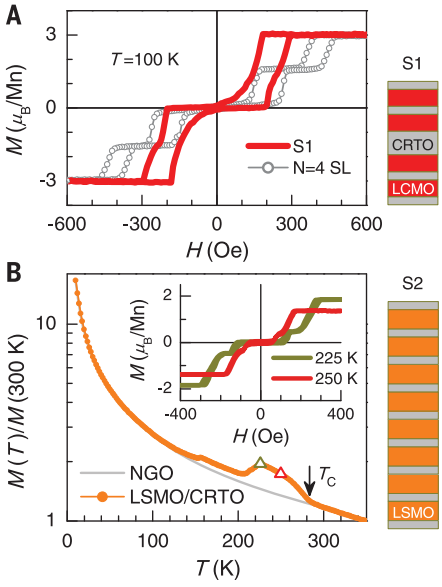

Fig. 4. Variations on the AF-IEC system based on the CRTO spacer. (**A**) *M-H* loops measured at 100 K from the N = 4 SL $[2.8/1.2]_4$ and the modified structure S1. The latter can be regarded as two N = 2 SLs connected by a thick CRTO spacer. (**B**) Normalized *M-T* curve measured from the LSMO/CRTO SL (S2), $[3.2/1.2]_8$, with a cooling field of 300 Oe applied along the in-plane [010] axis. The inset shows the loops measured at 225 and 250 K (as denoted in the *M-T* curve), respectively, with the paramagnetic background from the NGO substrate subtracted.

exchange field of the interior LCMO layers (H_{ex2} = 150 Oe). This means the magnetic reversal of each LCMO layer tends to adopt a spin-flip mode, as manifested by the sharp steplike switching (*11*). On the basis of all the loops (Fig. 3A and fig. S10), magnetic configurations at various temperatures and magnetic fields are mapped in Fig. 3B, and the coupling field H_{ex1} (H_{ex2}) and coercivity H_{C1} (H_{C2}) corresponding to the outer (interior) LCMO layers at various temperatures are also extracted (Fig. 3C). As the temperature is reduced, H_{ex1} (H_{ex2}) increases almost linearly and then saturates at lower temperatures, but H_{C1} (H_{C2}) increases exponentially in the whole temperature range. The different dependences of H_{ex1} and H_{C1} lead to a crossover from the AF state to the IS at ~50 K (Fig. 3B): At temperatures below 50 K, the MA energy increases more rapidly than the IEC strength (*35*), i.e., the IEC alone is unable to switch the outer LCMO layer without the help of a field applied in the reverse direction (fig. S11). At high temperatures, however, the coupling strength is greatly suppressed (Fig. 3C). This is in contradiction to the positive temperature coefficient predicted for IEC with an insulating spacer, where the charge carriers are thermally populated (*6*). However, it is consistent with the impurity-assisted IEC model previously mentioned. For the localized impurity states, the resonant character and the thermal broadening of the Fermi distribution will make the AF-IEC monotonically decrease with temperature (*33*). We believe that such an effect could also be overwhelmed by the greatly reduced magnetization especially near the T_C of LCMO layers in the system (figs. S10 and S12), because the magnetic excitations of the coupled FM layers usually play a dominant role in the temperature dependence of IEC (*36*).

So far, we have demonstrated AF-IEC with layer-resolved magnetic switching for LCMO/CRTO SLs. The results are highly reproducible, and moreover we find that the AF-IEC is tunable via the Ti-doping level of the CRTO spacer and the growth orientations (fig. S13). The multiple control of T_C, MA, interfacial octahedral connectivity, IEC, spin-dependent transport, and possibly the dimensionality effect (*15*, *16*) makes this epitaxial system rather intriguing, encouraging more detailed spectroscopic and theoretical studies on the spacers and interfaces, including the interfacial magnetism (*37*–*40*). We also show how our system can be extended for possible applications. First, we modify the N = 4 SL structure by increasing the layer thickness of only the central CRTO from y = 1.2 to 3.6 (denoted as S1). As shown in Fig. 4A, in contrast to the N = 4 SL, this structure maintains the remanent AF state, but the magnetization plateaus at ~ $\pm 1/2M_S$ disappear. This indicates that a thicker central CRTO layer can magnetically decouple the top and bottom N = 2 S-AFMs very effectively. Similarly, a further stack of the N = 2 SLs can progressively enhance the M_S at a moderate field but keep the stray field negligible, properties that are deemed highly desirable for biotechnology applications (*41*). Second, we fabricate the S-AFMs with SLs (S2) composed of CRTO and $La_{2/3}Sr_{1/3}MnO_3$ (LSMO) layers, another prototype manganite having a T_C (bulk) of 370 K. As shown in Fig. 4B, aside from a T_C of 286 K, a drop in magnetization at 227 K and the separated hysteresis loops with magnetization plateaus at ~ $\pm 1/4M_S$ (N = 8, inset) all signify the existence of AF-IEC in this SL, further underlining that the present S-AFMs are attractive for spintronic applications.

REFERENCES AND NOTES

1. S. A. Wolf *et al.*, *Science* **294**, 1488–1495 (2001).
2. S. Loth, S. Baumann, C. P. Lutz, D. M. Eigler, A. J. Heinrich, *Science* **335**, 196–199 (2012).
3. P. Wadley *et al.*, *Science* **351**, 587–590 (2016).
4. T. Jungwirth, X. Marti, P. Wadley, J. Wunderlich, *Nat. Nanotechnol.* **11**, 231–241 (2016).
5. M. D. Stiles, *J. Magn. Magn. Mater.* **200**, 322–337 (1999).
6. P. Bruno, *Phys. Rev. B Condens. Matter* **52**, 411–439 (1995).
7. J. Faure-Vincent *et al.*, *Phys. Rev. Lett.* **89**, 107206 (2002).
8. S. G. E. te Velthuis, J. S. Jiang, S. D. Bader, G. P. Felcher, *Phys. Rev. Lett.* **89**, 127203 (2002).
9. O. Hellwig, A. Berger, E. E. Fullerton, *Phys. Rev. Lett.* **91**, 197203 (2003).
10. S.-H. Yang, K.-S. Ryu, S. Parkin, *Nat. Nanotechnol.* **10**, 221–226 (2015).
11. R. Lavrijsen *et al.*, *Nature* **493**, 647–650 (2013).
12. A. Orozco *et al.*, *Phys. Rev. Lett.* **83**, 1680–1683 (1999).
13. K. R. Nikolaev *et al.*, *Phys. Rev. Lett.* **85**, 3728–3731 (2000).
14. W. M. Lü *et al.*, *Nat. Commun.* **7**, 11015 (2016).
15. M. Gibert *et al.*, *Nat. Commun.* **7**, 11227 (2016).
16. H. Y. Hwang *et al.*, *Nat. Mater.* **11**, 103–113 (2012).
17. H. Yamada *et al.*, *Science* **305**, 646–648 (2004).
18. E. J. Moon *et al.*, *Nano Lett.* **14**, 2509–2514 (2014).
19. M. Ziese, F. Bern, E. Pippel, D. Hesse, I. Vrejoiu, *Nano Lett.* **12**, 4276–4281 (2012).
20. B. B. Chen *et al.*, *Appl. Phys. Lett.* **104**, 242416 (2014).
21. P. F. Chen *et al.*, *Appl. Phys. Lett.* **103**, 262402 (2013).
22. J.-H. Park *et al.*, *Nature* **392**, 794–796 (1998).
23. M. Bowen *et al.*, *Appl. Phys. Lett.* **82**, 233–235 (2003).
24. T. He, R. J. Cava, *Phys. Rev. B* **63**, 172403 (2001).
25. See supplementary materials.
26. J. H. Song *et al.*, *Phys. Rev. B* **72**, 060405 (2005).
27. H. Boschker *et al.*, *Phys. Rev. B* **79**, 214425 (2009).
28. M. Charilaou, C. Bordel, F. Hellman, *Appl. Phys. Lett.* **104**, 212405 (2014).
29. S. S. P. Parkin, *Phys. Rev. Lett.* **67**, 3598–3601 (1991).
30. O. Hellwig, T. L. Kirk, J. B. Kortright, A. Berger, E. E. Fullerton, *Nat. Mater.* **2**, 112–116 (2003).
31. S. S. P. Parkin, A. Mansour, G. P. Felcher, *Appl. Phys. Lett.* **58**, 1473–1475 (1991).
32. B. Li *et al.*, *Appl. Phys. Lett.* **109**, 152401 (2016).
33. M. Ye. Zhuravlev, E. Y. Tsymbal, A. V. Vedyayev, *Phys. Rev. Lett.* **94**, 026806 (2005).
34. Z. Q. Qiu, J. Pearson, S. D. Bader, *Phys. Rev. B Condens. Matter* **46**, 8659–8662 (1992).
35. P. Poulopoulos, U. Bovensiepen, M. Farle, K. Baberschke, *Phys. Rev. B* **57**, R14036 (1998).
36. K. M. Döbrich *et al.*, *Phys. Rev. Lett.* **100**, 227203 (2008).
37. J. D. Hoffman *et al.*, *Phys. Rev. X* **6**, 041038 (2016).
38. B. R. K. Nanda, S. Satpathy, M. S. Springborg, *Phys. Rev. Lett.* **98**, 216804 (2007).
39. K. Terai *et al.*, *Phys. Rev. B* **77**, 115128 (2008).
40. J. W. Freeland *et al.*, *Phys. Rev. B* **81**, 094414 (2010).
41. T. Vemulkar, R. Mansell, D. C. M. C. Petit, R. P. Cowburn, M. S. Lesniak, *Appl. Phys. Lett.* **107**, 012403 (2015).

ACKNOWLEDGMENTS

We thank D. C. Meng, L. J. Zhang, W. S. Yan, and G. B. Zhang for experimental assistance and K. Yang, G. Cao, and Y. H. Zhang for helpful discussions. This work has been supported by the National Natural Science Foundation of China (grants 11474263, 11574281, and U1432251), the National Basic Research Program of China (grants 2015CB921201 and 2016YFA0401003), and the Hefei Science Center of the Chinese Academy of Sciences (grant 2016HSC-IU006).

SUPPLEMENTARY MATERIALS

www.sciencemag.org/content/357/6347/191/suppl/DC1
Materials and Methods
Figs. S1 to S13
References (*42*, *43*)

22 September 2016; accepted 7 June 2017
10.1126/science.aak9717

Downloaded from http://science.sciencemag.org/ on April 23, 2020

Science

All-oxide–based synthetic antiferromagnets exhibiting layer-resolved magnetization reversal

Binbin Chen, Haoran Xu, Chao Ma, Stefan Mattauch, Da Lan, Feng Jin, Zhuang Guo, Siyuan Wan, Pingfan Chen, Guanyin Gao, Feng Chen, Yixi Su and Wenbin Wu

Science **357** (6347), 191-194.
DOI: 10.1126/science.aak9717

Making an oxide-layered antiferromagnet

Antiferromagnetism, a state of matter where ordered neighboring spins point in opposite directions, can be engineered in layered heterostructures, which affords control over their properties. Doing so in oxide heterostructures is tricky because the necessary ferromagnetism of the constituent layers may not survive thinning to nanometer thicknesses. Chen *et al.* overcame this materials challenge by finding and growing the right combination of substrate, magnetic, and insulating layers to engineer antiferromagnetic coupling. The resulting superlattices, consisting of alternating layers of a ferromagnetic oxide and an insulating material, exhibit layer-by-layer switching of magnetization.

Science, this issue p. 191

ARTICLE TOOLS http://science.sciencemag.org/content/357/6347/191

SUPPLEMENTARY MATERIALS http://science.sciencemag.org/content/suppl/2017/07/12/357.6347.191.DC1

REFERENCES This article cites 42 articles, 4 of which you can access for free
http://science.sciencemag.org/content/357/6347/191#BIBL

PERMISSIONS http://www.sciencemag.org/help/reprints-and-permissions

Use of this article is subject to the Terms of Service

Science (print ISSN 0036-8075; online ISSN 1095-9203) is published by the American Association for the Advancement of Science, 1200 New York Avenue NW, Washington, DC 20005. The title *Science* is a registered trademark of AAAS.

Copyright © 2017 The Authors, some rights reserved; exclusive licensee American Association for the Advancement of Science. No claim to original U.S. Government Works

Downloaded from http://science.sciencemag.org/ on April 23, 2020